Table 4 Scalability test: cold test, one-block grids, 1500 iterations

No. of processors	Time, s		
	1025 × 65 points	513 × 65 points	257 × 65 points
1	—	—	917
2	—	926	466
4	944	480	262
8	506	267	226
16	342	203	—
32	296	—	—

masked blocks is made only if the difference between the averaged computational load and the one performed by one of the processors is higher than a fixed percentage (20% for these calculations).

Finally, some more tests have been made to check the scalability. Such tests cannot be made easily on the hot case, because on increasing the numbers of points, the computational load does not rise proportionally, since the ratio between the numbers of points with a temperature higher and lower than the limit temperature generally varies. Therefore, the test has been made only on the cold case, on a one-block grid. The computations have been performed at three grid levels: grid 1, 257 × 65; grid 2, 513 × 65; and grid 3, 1025 × 65. The results are shown in Table 4, in which the scalability can be seen to be generally good.

Conclusions

A hypersonic Navier–Stokes nonequilibrium code has been parallelized using the masked MBT with an automatic load-balancing algorithm. A number of tests have been made over a double ellipse; the original grid consisted of seven blocks, each one with a different number of points. Balancing is automatically controlled during the computation to take into account the different load due to the chemical terms. The results show good efficiency, particularly over the fine grid. The effect of dynamic balancing is also significant for these cases.

Other applications of the algorithm are under test: in particular, local grid refinement is being extended to the parallel version. Furthermore, it could be convenient to make a check to recognize the points where the computation can be avoided (i.e., the freestream points far enough from the shock wave); in that case the automatic load balancing would be very useful. Finally, it can be said that the procedure used seems to be fundamental in all the future applications of this code, if flowfields over greater grids (e.g., three-dimensional cases) are to be computed.

References

[1]Borrelli, S., and Pandolfi, M.,"An Upwind Formulation for the Numerical Prediction of Nonequilibrium Hypersonic Flows," *Proceedings of 12th International Conference on Numerical Methods in Fluid Dynamics* (Oxford, England, UK), edited by J. W. Morton, Springer–Verlag, 1990, pp. 416–420.

[2]Borrelli, S., and Schettino, A., "Influence of Chemical Modelling on Hypersonic Flow," *Proceedings of First European Symposium on Aerothermodynamics for Space Vehicles*, edited by B. Battrick, SP-318.23, European Space Agency, European Space Research and Technology Centre, 1991, pp. 335–341.

[3]Schettino, A., Borrelli, S., and De Filippis, F., "Influence of Transport and Thermokinetic Models in Free-Flight and in Plasma Wind Tunnel Tests," *Proceedings of the 5th International Symposium on Computational Fluid Dynamics* (Sendai, Japan), edited by H. Daiguji, Japan Society of Computational Fluid Dynamics, 1993, pp. 75–80.

[4]Borrelli, S., and Schiano, P., "A Nonequilibrium Hypersonic Flow Calculation on a Massively Parallel Computer," *Proceedings of Parallel CFD 1991* (Stuttgart, Germany), edited by K. G. Reinsch et al., Elsevier, Amsterdam, 1991, pp. 59–73.

[5]Borrelli, S., Matrone, A., and Schiano, P., "A Multiblock Hypersonic Flow Solver for a Massively Parallel Computer," *Proceedings of Parallel CFD 1992* (New Brunswick, NJ), edited by R. B. Pelz, A. Ecer, and J. Hauser, Elsevier, Amsterdam, 1992, pp. 25–37.

[6]Geist, A., Beguelin, A., Dongarra, J., Jiang, W., Manchek, R., and Sunderam, V., *PVM, Parallel Virtual Machine. A User's Guide and Tutorial for Networked Parallel Computing*, MITT Press, London, 1994.

I. D. Boyd
Associate Editor

Lower–Upper Symmetric Gauss–Seidel Scheme Exhibiting Asymmetric Vortices over Slender Bodies

Soo Jung Hwang* and Oh Hyun Rho†
Seoul National University,
Seoul 151-742, Republic of Korea

Nomenclature

$\hat{A}, \hat{B}, \hat{C}$	= Jacobian matrix of convective flux vectors
C_Y	= side-force coefficient, side force/$[q\pi D^2/4]$
D	= cylinder diameter
$D_\xi^+, D_\eta^+, D_\zeta^+$	= forward difference operators
$D_\xi^-, D_\eta^-, D_\zeta^-$	= backward difference operators
$\hat{E}, \hat{F}, \hat{G}$	= convective flux vectors
$\hat{G}_v$	= viscous flux vector in radial coordinate ζ
I	= identity matrix
J	= Jacobian of transformation
M_∞	= freestream Mach number
$\hat{Q}$	= conserved variable vector
q_∞	= freestream dynamic pressure
$\hat{R}$	= residual vector
Re_D	= Reynolds number based on cylinder diameter
t, τ	= time
x, y, z	= Cartesian coordinates
α	= angle of attack
Δ	= correction $()^{n+1} - ()^n$, where n denotes time level
ξ, η, ζ	= generalized curvilinear coordinates in the streamwise, circumferential, and radial direction.

Introduction

A PERFECT numerical simulation of asymmetric vortical flow around slender bodies at high angle of attack, which was observed experimentally,[1,2] is extremely difficult to obtain accurately. One of the difficulties lies in that it suffers from numerical errors inherently induced in the process of computation. Earlier researchers found out experimentally,[1,2] as well as numerically,[3–9] that minute asymmetric disturbance might cause large asymmetry in the entire flowfield. Siclari and Marconi[5] demonstrated asymmetric flow solutions by solving Navier–Stokes equations with conical assumptions obtained without preimposing any perturbation. A recent numerical study by Levy et al.[9] indicated that asymmetric errors introduced in the diagonalization process developed a spurious asymmetry in the flow.

A consequence of the previous results has been the assumption that the steady-state solution that depends only on the right-hand side of the algorithm, which has been generally accepted, does not hold for the high angle-of-attack flows. In this Note, a recently developed lower–upper symmetric Gauss-Seidel (LU-SGS)[10] algorithm, has been applied without introducing any perturbation intentionally. The scheme does not symmetrically factorize the flux Jacobian of the left-hand side. Asymmetric vortical flows have been obtained numerically[11,12] simply through direct application of LU-SGS scheme. The origin of the numerical asymmetry has also been investigated.

Received May 30, 1995; presented as Paper 95-1799 at the AIAA 13th Applied Aerodynamics Conference, San Diego, CA, June 19–22, 1995; revision received March 15, 1996; accepted for publication May 3, 1996.

*Graduate Research Assistant, Department of Aerospace Engineering.
†Professor, Department of Aerospace Engineering. Member AIAA.

Numerical Algorithms

The governing equations are the three-dimensional, time-dependent, and compressible thin-layer Navier–Stokes equations, which are written in conservation form with generalized coordinates as follows[11,12]:

$$\partial_\tau \hat{Q} + \partial_\xi \hat{E} + \partial_\eta \hat{F} + \partial_\zeta (\hat{G} - \hat{G}_v) = 0 \tag{1}$$

These equations are solved with finite volume method for both steady and unsteady flow. The convective and pressure terms are upwind differenced by application of Roe's[13] flux difference splitting scheme, whereas the shear stress and heat transfer terms are centrally differenced.

Yoon and Jameson[10] introduced an implicit algorithm based on a lower–upper factorization and Gauss-Seidel relaxation. Because the LU-SGS scheme does not require additional relaxation of factorization on planes of sweep, it can reduce memory and computation time required for three-dimensional computation. The LU-SGS scheme can be written as

$$(LD^{-1}U)\Delta\hat{Q} = -\hat{R} \tag{2}$$

where

$$\begin{aligned} L &= I/J\Delta t + D_\xi^- \hat{A}^+ + D_\eta^- \hat{B}^+ + D_\zeta^- \hat{C}^+ - \hat{A}^- - \hat{B}^- - \hat{C}^- \\ D &= I/J\Delta t + \hat{A}^+ - \hat{A}^- + \hat{B}^+ - \hat{B}^- + \hat{C}^+ - \hat{C}^- \\ U &= I/J\Delta t + D_\xi^+ \hat{A}^- + D_\eta^+ \hat{B}^- + D_\zeta^+ \hat{C}^- + \hat{A}^+ + \hat{B}^+ + \hat{C}^+ \\ \hat{R} &= -(I/J\Delta t)^2 [D_\xi \hat{E} + D_\eta \hat{F} + D_\zeta (\hat{G} - \hat{G}_v)] \end{aligned} \tag{3}$$

The Jacobian matrices of the flux vectors are approximately constructed to yield diagonal dominance:

$$\hat{A}^\pm = \frac{\hat{A} \pm \rho(\hat{A})I}{2} \quad \text{and} \quad \rho(\hat{A}) = \beta \max[|\lambda(\hat{A})|] \tag{4}$$

where $\lambda(\hat{A})$ represents eigenvalue of Jacobian matrix $\hat{A}$ and β is a constant that is greater than or equal to 1.

The preceding factored equation is solved as a series of following lower and upper sweeps

$$L\Delta\hat{Q}^* = \hat{R} \tag{5}$$

$$U\Delta\hat{Q} = D\Delta\hat{Q}^* \tag{6}$$

and vectorized on $i + j + k = \text{const}$ oblique planes of sweep.

Two-point one-sided differences reduce Eq. (3) to

$$\begin{aligned} L &= I/J\Delta t + \rho - \hat{A}^+_{i-1,j,k} - \hat{B}^+_{i,j-1,k} - \hat{C}^+_{i,j,k-1} \\ D &= I/J\Delta t + \rho \\ U &= I/J\Delta t + \rho + \hat{A}^-_{i+1,j,k} + \hat{B}^-_{i,j+1,k} + \hat{C}^-_{i,j,k+1} \end{aligned} \tag{7}$$

where $\rho = \rho(\hat{A}) + \rho(\hat{B}) + \rho(\hat{C})$.

In the inversion process, $\hat{A}^+_{i-1,j,k}$, $\hat{B}^+_{i,j-1,k}$, and $\hat{C}^+_{i,j,k-1}$ are multiplied by $\Delta\hat{Q}^*_{i-1,j,k}$, $\Delta\hat{Q}^*_{i,j-1,k}$, and $\Delta\hat{Q}^*_{i,j,k-1}$, respectively, and handled explicitly to permit scalar diagonal inversion. The use of approximate flux Jacobian in Eq. (4) with a shorter computation time per iteration introduces directional characteristics for the sweeping plane, which are mainly contributed by the terms of $\hat{B}$ and $\hat{C}$ in Eq. (7). Although the directional characteristics has been known to have no influence on the steady-state solution in many aerodynamic problems, it may affect the numerical solutions for the flow regimes at high angle of attack where asymmetry was experimentally observed.

Results and Discussion

Computations have been performed based on LU-SGS algorithm for subsonic flow of $M_\infty = 0.2$ over an ogive-cylinder body, which consisted of a 3.5 diameter tangent ogive forebody with an 8.5 diameter cylindrical afterbody extending aft of the nose–body junction to $x/D = 12$. This body geometry has been experimentally tested by Lamont[1] extensively. The grid consists of 90 circumferential planes extending completely around the body. In each circumferential plane, the grid contains 50 radial points between the body surface and the computational outer boundary, and 45 axial points between the nose and the rear of the body. The crossflow plane grid is exactly symmetric between left and right sides.

An adiabatic no-slip boundary condition is applied at the body surface and the characteristic boundary condition is maintained at the computational outer boundary. A nonreflecting boundary condition is applied at the downstream boundary.

Figure 1 shows the histories of computed side force coefficients for the steady and unsteady cases. Computations were carried out for Re_D of 2.0×10^5, $M_\infty = 0.2$, and $\alpha = 40$ deg. Steady and unsteady (time-accurate) converged solutions are asymmetric. Although the unsteady solution has smaller fluctuations in the early stages than the steady solution, two converged side force values finally coincide with each other.

Figure 2 shows the computed total pressure contours at several cross sections along the body. The solution shows large asymmetric vortices around the aft part of the body. The asymmetric solution may be caused by its own asymmetric sweeping property. For example, in the lower sweeping process in Eq. (5), the unknown $\Delta\hat{Q}^*$ is computed exclusively through residual and prior information during computation in the direction of sweep and vice versa. This directional computational nature may be characterized by introduction of asymmetric numerical errors for the crossflow plane and develops the flow into an asymmetric steady-state solution. Therefore, the LU-SGS scheme can be classified as an asymmetric algorithm. The details are described in Refs. 11 and 12.

Figure 3 shows the top view of the skin friction lines. The separation lines are not symmetric to the leeward side, and a large asymmetry can be clearly seen aft of the cylinder body.

Figure 4 shows the crossflow streamlines at several cross sections. The alternating periodic shedding of the vortices at the body surface can be seen clearly.

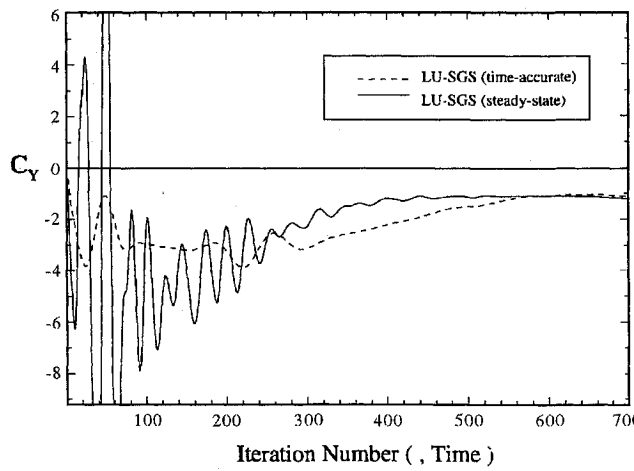

Fig. 1 Side force coefficient histories: $M_\infty = 0.2$, $\alpha = 40$ deg, and $Re_D = 2.0 \times 10^5$.

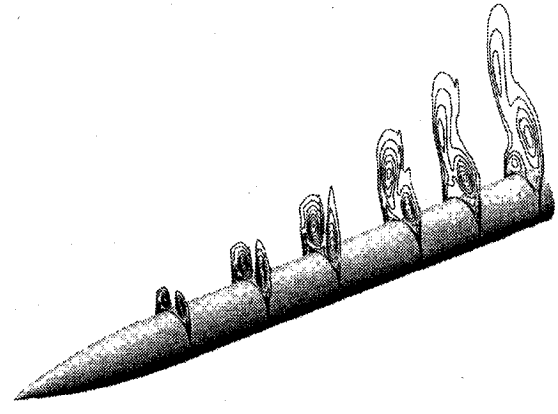

Fig. 2 Total pressure contours at several cross sections: $M_\infty = 0.2$, $\alpha = 40$ deg, and $Re_D = 2.0 \times 10^5$.

Fig. 3 Skin friction lines: M_∞ =0.2, α = 40 deg, and $Re_D = 2.0 \times 10^5$.

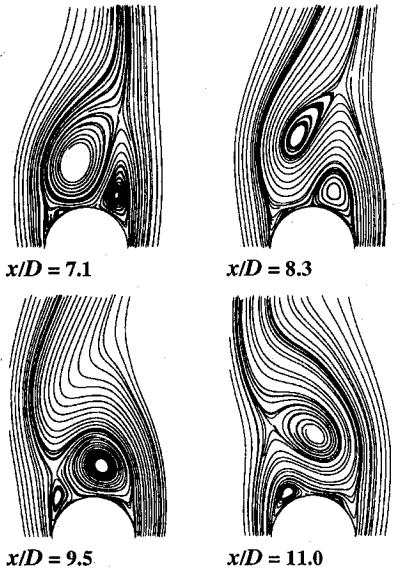

Fig. 4 Crossflow streamlines on several cross sections: M_∞ = 0.2, α = 40 deg, and $Re_D = 2.0 \times 10^5$.

Conclusion

The simply direct application of LU-SGS algorithm without introduction of any asymmetric perturbation yields an asymmetric solution. It may be a result of the directional characteristics of the scheme.

References

[1]Lamont, P. J., "The Complex Asymmetric Flow over a 3.5*D* Ogive Nose and Cylindrical Afterbody at High Angles of Attack," AIAA Paper 82-0053, Jan. 1982.

[2]Zilliac, G. G., Degani, D., and Tobak, M., "Asymmetric Vortices on a Slender Body of Revolution," *AIAA Journal*, Vol. 29, No. 5, 1991, pp. 667–675.

[3]Degani, D., "Effect of Geometrical Disturbance on Vortex Asymmetry," *AIAA Journal*, Vol. 29, No. 4, 1991, pp. 560–566.

[4]Degani, D., and Schiff, L. B., "Numerical Simulation of the Effect of Spatial Disturbances on Vortex Asymmetry," *AIAA Journal*, Vol. 29, No. 3, 1991, pp. 344–352.

[5]Siclari, M. J., and Marconi, F., "The Computation of Navier–Stokes Solutions Existing Asymmetric Vortices," AIAA Paper 89-1817, June 1989.

[6]Hartwich, P. M., Hall, R. M., and Hemsch, M. J., "Navier–Stokes Computations of Vortex Asymmetries Controlled by Small Surface Imperfections," AIAA Paper 90-0385, Jan. 1990.

[7]Vanden, K. J., and Belk, D. M., "Numerical Investigation of Subsonic and Supersonic Asymmetric Vortical Flow," AIAA Paper 91-2869, 1991.

[8]Thomas, J. L., "Reynolds Number Effects on Supersonic Asymmetrical Flows over a Cone," *Journal of Aircraft*, Vol. 30, No. 4, 1993, pp. 488–495.

[9]Levy, Y., Hesselink, L., and Degani, D., "Anomalous Asymmetries in Flows Generated by Algorithms that Fails to Conserve Symmetry," *AIAA Journal*, Vol. 33, No. 6, 1995, pp. 999–1007.

[10]Yoon, S., and Jameson, A., "Lower–Upper Symmetric-Gauss-Seidel Method for the Euler and Navier–Stokes Equations," *AIAA Journal*, Vol. 26, No. 9, 1988, pp. 1025, 1026.

[11]Hwang, S. J., "Effect of Numerical Schemes on Predicting the Flow Phenomena Around a Slender Body at High Angle of Attack," Ph.D. Thesis, Dept. of Aerospace, Seoul National Univ., Seoul, Republic of Korea, Feb. 1996.

[12]Rho, O. H., and Hwang, S. J., "Numerical Simulation of Asymmetric Vortical Flows on a Slender Body at High Incidence," AIAA Paper 95-1799, June 1995.

[13]Roe, P. L., "Approximate Riemann Solvers, Parameter Vectors and Difference Schemes," *Journal of Computational Physics*, Vol. 43, 1983, pp. 357–372.

R. M. Cummings
Associate Editor

Dual Fuel Solar Thermal Stage: Ideal Analysis

Jesse F. Stewart*
University of Washington, Seattle, Washington 98195-2250
and
James A. Martin†
University of Alabama, Tuscaloosa, Alabama 35487-0280

Introduction

SOLAR thermal propulsion is a concept that makes use of the sun's energy to heat a working fluid as a means of providing thrust. The thrust is generated by expanding a superheated fluid through a nozzle. Although the term burn is used throughout this Note, no combustion actually occurs. Because the thrust level generated is relatively low, the solar thermal concept can only be used as an upper stage to provide orbital transfers. Most of the solar thermal systems currently being studied use a single fuel, such as liquid hydrogen. However, there are problems with these systems such as small payload volume, significant propellant losses, and large, expensive power systems. One possible solution to these problems is the development of a dual fuel solar thermal engine. This Note reports the initial stages of work on such a system. The dual fuel engine is designed to use ammonia (NH_3) and hydrogen (H_2) during specific stages of the transfer mission, from low Earth orbit (LEO) to geosynchronous equatorial orbit (GEO), in an attempt to overcome the shortcomings of a hydrogen only system.

The work is based on a solar thermal engine system reported in Ref. 1. The system in Ref. 1 uses hydrogen to produce a specific impulse of 860 s and a thrust level of 2 lbf. Two parabolic collectors are mounted on a rotation and gimbal system and are inflated after separation of the upper stage from the launch vehicle. The collectors focus sunlight into a blackbody absorber cavity and raise the temperature of the walls. This heat is transferred to liquid hydrogen flowing through preheater tubes that encircle the absorber. The hydrogen then passes into the absorber, is superheated, and expands through the nozzle to generate thrust.

Ideal Rocket Analysis

The basic characteristics of the system were modeled using data from Ref. 1 and the ideal rocket equation.[2] The ideal rocket analysis was performed using a computer program that calculated the component weights of the system. An ideal velocity change for a transfer from a LEO altitude of 400 nm to GEO altitude was calculated from a gross weight of 5400 lb and a fuel weight, without losses, of 2140 lb as given in the feasibility report.[1] Losses were included to account for boil off, startup and shutdown, leakage, residuals and plume impingement, and extra fuel reserves, all of which brought the total propellant weight to 2696 lb. The tank weight was calculated as 15% of the hydrogen weight. The component weights yielded a dry weight of 1721 lb. These weights resulted in a payload weight of 983 lb. These results were within ±3% of the data in Ref. 1. This system was used as a baseline to develop a dual fuel system.

There are possible advantages to developing a dual fuel solar thermal engine. By using hydrogen and a heavier fuel such as ammonia, tank volume and tank weight can be decreased significantly from that required for a system using only hydrogen. This volume decrease allows the spacecraft to carry a larger payload. Propellant

Received June 2, 1995; revision received March 9, 1996; accepted for publication March 28, 1996.

*Graduate Student, Department of Aeronautics and Astronautics. Student Member AIAA.

†Associate Professor, Aerospace Engineering. Associate Fellow AIAA.